Journal of Hazardous Materials 162 (2009) 161–173

Contents lists available at ScienceDirect

Journal of Hazardous Materials

journal homepage: www.elsevier.com/locate/jhazmat

SEM/EDS and XRD characterization of raw and washed MSWI fly ash sintered at different temperatures

Yangsheng Liu[a,b,c,*], Liting Zheng[a,b], Xiaodong Li[a,c], Shaodong Xie[a]

[a] College of Environmental Science and Engineering, Peking University, Beijing 100871, China
[b] The Key Lab of Water and Sediment Sciences, Ministry of Education, Beijing 100871, China
[c] Peking University Shenzhen Graduate School, Shenzhen 518057, China

ARTICLE INFO

Article history:
Received 31 August 2007
Received in revised form 27 March 2008
Accepted 5 May 2008
Available online 13 May 2008

Keywords:
Fly ash
Toxicity characteristic leaching procedure (TCLP)
Heavy metals
Sintering

ABSTRACT

The disposal of fly ash generated during municipal solid waste incineration (MSWI) may pose a significant risk to the environment due to the possible leaching of hazardous pollutants, such as toxic metals. Sintering technology attracted more attention than the vitrification process because of its low energy needed. Generally, a preliminary washing treatment of raw fly ash with water was necessary for this sintering technology. This study investigated the composition and morphology of raw fly ash (RFA) and washed fly ash (WFA) at different sintering temperatures, and examined the newly formed minerals during sintering. Toxicity characteristic leaching procedure (TCLP) tests were carried out to investigate the effect of the washing treatment and sintering process on the leaching performance of heavy metals in fly ash. Results showed that, with an increase of sintering temperature more complex aluminosilicates were formed; the incorporation of Mg, Fe and Pb into the aluminosilicates occurred during the sintering process at higher temperatures (800 and 900 °C). The washing treatment reduced the leachable concentration of Cd, Pb and Ni, but increased that of Cr. A $CaCrO_4$ compound was considered as a potential soluble species.

1. Introduction

Incineration is an efficient method for municipal solid wastes (MSW) treatment, achieving up to a 90% volume reduction, a 60–75% mass reduction, a destruction of pathogenic agents and a possible recovery of energy. Among the solid residues generated from MSW incineration, fly ash is regarded as a very toxic material owing to its high concentration of leachable heavy metals and, in some cases, to the presence of chlorinated organic compounds. The results of leaching tests for fly ash show that the concentration of some elements, usually heavy metals including Cd, Cr, Zn, etc., exceeds the regulatory limits [1] and cannot be disposed of in the present form and therefore require a stabilization or inertisation treatment prior to disposal [2]. Landfilling is a common practice for the disposal of fly ash currently, but it requires large areas which are not available for other human activities, so avoiding landfill disposal of fly ash by developing reuse applications is clearly the preferred option and has been the subject of extensive research [3–5].

In recent years, thermal treatment techniques such as vitrification and sintering have been proposed to convert fly ash into glass- and ceramic materials for re-utilization. Results from Park et al. [4] indicate that the vitrification technique is effective for the stabilization and recycling of toxic fly ash. This type of treatment allows the melted slag to be used as a resource (e.g., a non-ferrous smelting material) [6]. However, the vitrification technique seems to be too expensive due to the melting of fly ash at high temperature generally over 1300–1400 °C; additionally, the melting equipment needs to be improved for its refractory materials and the corrosion prevention performance due to the high chlorides levels in fly ash [6].

Recently, more attention is paid to the sintering technology, which is less expensive than vitrification because of its lower heating temperature. A lot of researches suggested that a preliminary washing treatment of raw fly ash with water represents a basic step for successful thermal processing of such a material [7–9]. The results from Wang et al. [8] indicate that calcium-containing aluminosilicates with a relatively low-melting point are newly formed in the residual ash during the water extraction process, which are thought to contribute to the heavy metal stability in the washed ash, through binding mechanism in the silicate structure. Additionally, Cr behaves quite differently from the other heavy metals such as Cu, Cd and Pb during the toxicity characteristic leaching procedure (TCLP) tests for unwashed fly ash and washed fly ash at

* Corresponding author at: College of Environmental Science and Engineering, Peking University, Beijing 100871, China. Fax: +86 10 62751756.
E-mail addresses: yshliu@pku.edu.cn, liu_ysh@263.net (Y. Liu).

0304-3894/$ – see front matter © 2008 Elsevier B.V. All rights reserved.
doi:10.1016/j.jhazmat.2008.05.029

Table 1
Total composition of MSWI fly ash

Element	Concentration (mg kg^{-1})	S.D.[a]	Element	Concentration (mg kg^{-1})	S.D.[a]
Ca	233900	0.017	Sn	1070	0.005
Cl	158200	0.018	Ba	1010	0.005
Na	51500	0.09	Ce	594	0.0027
Sx	27200	0.05	Mn	435	0.0022
K	40600	0.09	La	396	0.0032
Si	20600	0.05	Sr	256	0.0013
Al	12600	0.04	Cd	252	0.001
Mg	10600	0.04	Ni	207	0.0012
Fe	10900	0.04	In	162	0.0009
Br	11100	0.05	Rb	140	0.0007
Zn	9043	0.041	Zr	109	0.0005
Cr	7040	0.04	Nd	89	0.0005
Px	3080	0.015	As	70	0.0018
Ti	2390	0.012	Pr	45	0.0017
Pb	3277	0.015	V	30	0.0004
Sb	2430	0.012	Mo	35	0.0005
F	1610	0.047	Bi	22	0.0005
Cu	1600	0.006			

[a] S.D.: standard error.

different sintering temperatures. The chromium (Cr) in the sintered ash becomes more readily leachable with increasing sintering time and temperature.

The objectives of this study are to investigate the effect of sintering temperature on the composition and morphology of raw fly ash (RFA) and washed fly ash (WFA), and to examine the newly formed minerals in RFA and WFA at different sintering temperatures, which account for the low leaching concentrations of heavy metals during the TCLP tests, and to give an explanation for the quite different behavior of Cr during the TCLP tests from a mineralogical point of view.

2. Materials and methods

2.1. Materials

The fly ash samples used in this study were collected from the baghouse of a mass-burn incinerator located in Shenzhen City of southern China. This incinerator has a capacity of 800 tons/day and is equipped with an air pollution control system consisting of three basic components: spray-dryer system, baghouse, and activated carbon adsorption column. In the spray-dryer system, the $Ca(OH)_2$ solution is atomized as small droplets (less than 30 μm in diameter) and sprayed into flue gas through a rotary atomizer to remove acid gases.

The fly ash taken from the baghouse was homogenized, then placed into a pan and oven dried at 105 °C ± 0.5 °C for 24 h. After the samples were dried and cooled, they were again ground and homogenized, and finally sieved. The fraction which passed through a #70 sieve was then analyzed to determine its principal properties.

2.2. Methods

The washing experiments were carried out with distilled water as the extractant, employing L/S ratio of 20, and extraction time of 60 min. the washing operation was described by Wang et al. [8]. After the washing process, the suspension was filtered in a vacuum and the filter cake was again washed twice. The resulting material was then oven dried at 105 °C ± 0.5 °C for 24 h, and then ground and desiccated. This dried material was labeled 'washed fly ash'.

In the sintering experiments, RFA and WFA were oven heated at 500, 600, 700, 800 and 900 °C for 1 h. Finally, RFA, WFA and their sintered products at different temperatures were subjected to analyses by virtue of scanning electron microscopy–energy dispersive spectroscopy (SEM–EDS) and X-ray powder diffraction (XRD). Before analyses, the sintered samples were ground to <150 μm.

The leachability of heavy metals (Cu, Cr, Cd, Pb, Zn and Ni) in RFA, WFA and their sintered products was evaluated by a toxicity characteristic leaching procedure according to the Chinese standard acetic acid leaching test, which was described in detail elsewhere [10].

2.3. Analysis

The elemental composition of RFA was determined by X-Ray Fluorescence Spectrometer (XRF) (ADVANT' XP+, Thermo Electron).

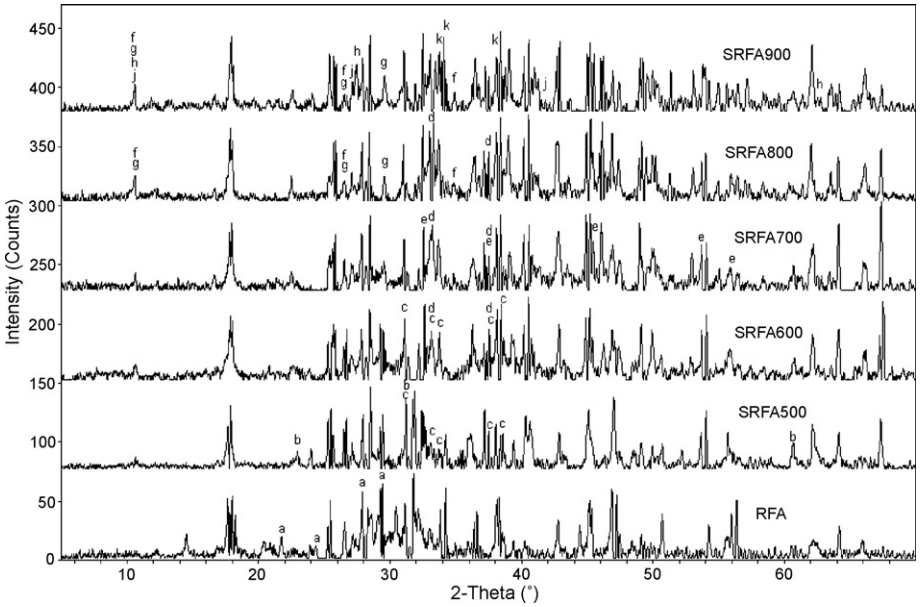

Fig. 1. XRD patterns of RFA powder and its sintered products. (a) Anorthite, (b) gehlenite, (c) zoisite, (d) grossular, (e) hibschite, (f) glaucophane, (g) cordierite, (h) ferroglaucophane, (j) ferrogedrite, (k) ferrotschermakite.

Table 2
XRD-based possible mineralogy of raw fly ash and sintered products

FRA		SRFA500		SRFA600		SRFA700		SRFA800		SRFA900	
Minerals	FOM	Minerals	FOM	Minerals	FOM	Minerals	FOM	Minerals	FOM	Minerals	FOM
Aluminosilicates											
Anorthite $CaAl_2Si_2O_8$	16.8	Gehlenite $Ca_2Al_2SiO_7$	14.7	Grossular $Ca_3Al_2(SiO_4)_2(OH)_4$	18.1	Grossular $Ca_3Al_2(SiO_4)_2(OH)_4$	16.7	Glaucophane $Na_2Mg_3Al_2Si_8O_{22}(OH)_2$	13.8	Glaucophane $Na_2Mg_3Al_2Si_8O_{22}(OH)_2$	13.3
		Zoisite $Ca_2Al_3Si_3O_{12}(OH)$	19.7	Zoisite $Ca_2Al_3Si_3O_{11}(O,OH)_2$	20.0	Hibschite $Ca_3Al_2(SiO_4)_{1.25}(OH)_7$	17.6	Grossular $Ca_3Al_2(SiO_4)_2(OH)_4$	15.6	Ferrotschermakite $Ca_2Fe_3Al_2(Si_6Al_6)O_{22}$-$(OH)_2$	16.0
								Cordierite $Mg_2Al_4Si_5O_{18}$	19.6	Ferroglaucophane $Na_2(Fe,Al,Mg)_5Si_8O_{22}$-$(OH)_2$	16.9
										Ferrogedrite $Fe_5Al_4Si_6O_{22}(OH)_2$	18.4
										Cordierite $Mg_2Al_4Si_5O_{18}$	19.8
Other major minerals											
AlO(OH)	10.1	$Ca_{1.5}SiO_{0.35}{\cdot}xH_2O$	4.9	$Al_2Si_2O_5(OH)_4$	3.5	Ca_2BO_3Cl	17.9	$Ca_3Mg(SiO_4)_2$	12.0	ZnSe	11.6
$CaSO_4$ (Anhydrite)	14.3	FeF_2	11.8	MgO	8.7	$Ca_{12}Al_{14}O_{32}Cl_2$	18.6	$Ca_{10}(SiO_4)_3(SO_4)_3Cl_2$	14.2	ZnS	13.5
CaClOH	15.0	CaO	14.7	$(MgO)_{0.91}FeO_{0.09}$	12.6	Ca_2PO_4Cl	19.2	$MgCO_3$	14.8	$Na_3Mg(CO_3)_2Cl$	14.7
$KCaCl_3$	16.4	$Ca_2ZnSi_2O_7$	15.0	ZnS	12.9	$Ca_2ZnSi_2O_7$	19.6	Ca_2PO_4Cl	16.5	$Ca_5(P,Si,S)_3O_{12}(Cl,OH,F)$	18.4
$(Mg,Cu)_2CO_3(OH)_2$	16.4	MgO	15.4	FeS_2	15.1	$MgCO_3$	19.8	$Ca_2ZnSi_2O_7$	18.8	$Ca_{9.983}(PO_4)_6Cl_{7.966}$	19.1
$MgAl_2(PO_4)_2(OH)_2$	16.4	$Ca_2Ti_5O_{12}$	15.6	CaClOH	15.8						
$Mg(ClO_2)_2{\cdot}6H_2O$	16.8	$Ca_5(PO_4)_3F$	16.6	$BaSiO_4$	15.8						
$Na_2H_2P_2O_7{\cdot}6H_2O$	16.9	$NaCaHSiO_4$	19.0	$Ca_2ZnSi_2O_7$	16.3						
$CaCl_2(H_2O)_4$	17.2	$K_6Al_2O_6$	19.8	$Ca_3Al_2O_6$	19.8						
$FeAl_2(PO_4)_2(OH)_2$	17.2	CaClOH	19.9	$NaCaPO_4$	19.8						
$Ca(OH)_2$	18.2										
NaCl	19.6										

Fig. 2. SEM image of RFA.

Crystalline phases present in RFA, WFA and their sintered products were analyzed by XRD (D/max2400, Rigaku) using 100 mA, and 40 kV, Cu K_α radiation. XRD analyses were run in three replicates. Scans were conducted from 5.00 to 70.00° at a rate of 0.5° 2θ/min. A PC-based search–match program, Jade 5.0 (Materials Data, Inc.), was used to identify possible crystalline phases in the powders, and figure of merit (FOM) was calculated based on weightings of 90% for peak location and 10% for peak intensity. Searches were based on PDF sets 1–54, 65, and 70–89. An FOM of 20 is considered a good fit, and an FOM of 10 is considered an excellent fit for these complex polycrystalline powders [11].

The determination of probable minerals in RFA, WFA and sintered products from the triplicate analyses was based on: (i) their presence in at least two of the three replicates, (ii) a figure of merit of 20 or less, and (iii) use of total compositional data and likely detection limits for XRPD [11]. The crystalline phase must have the possibility of having a concentration above some limit. For example,

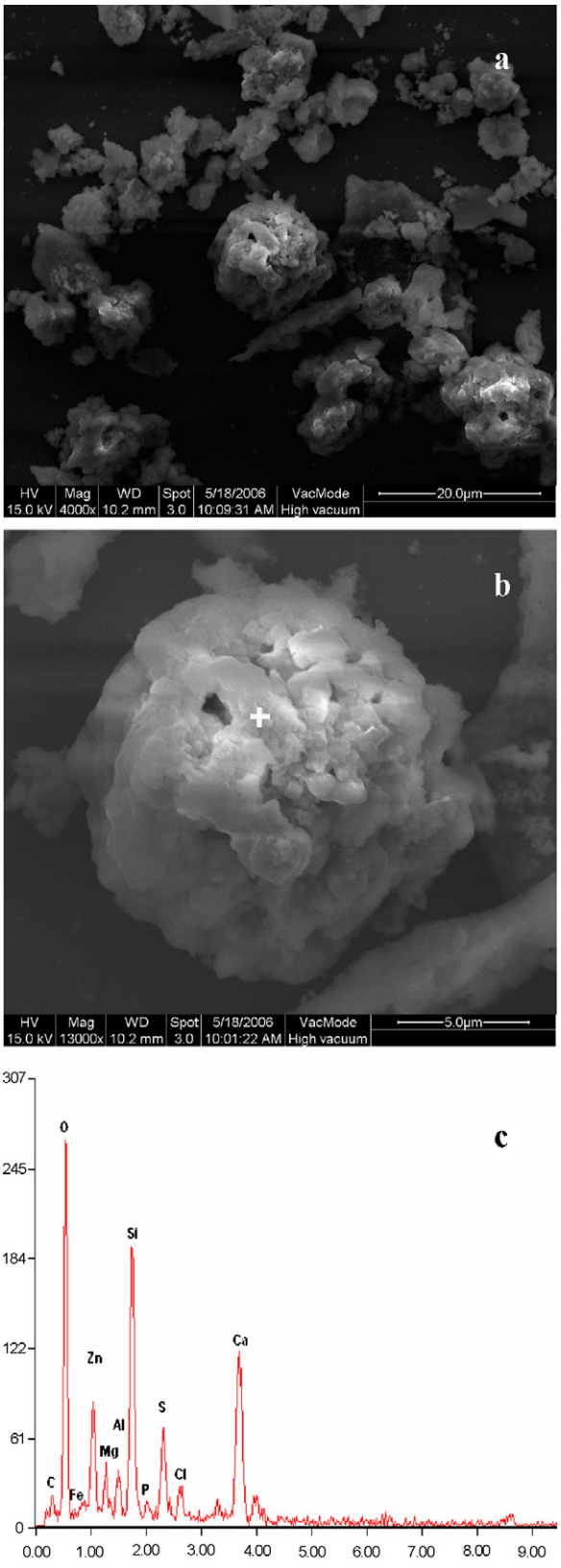

Fig. 3. SEM and EDS image of SRFA500.

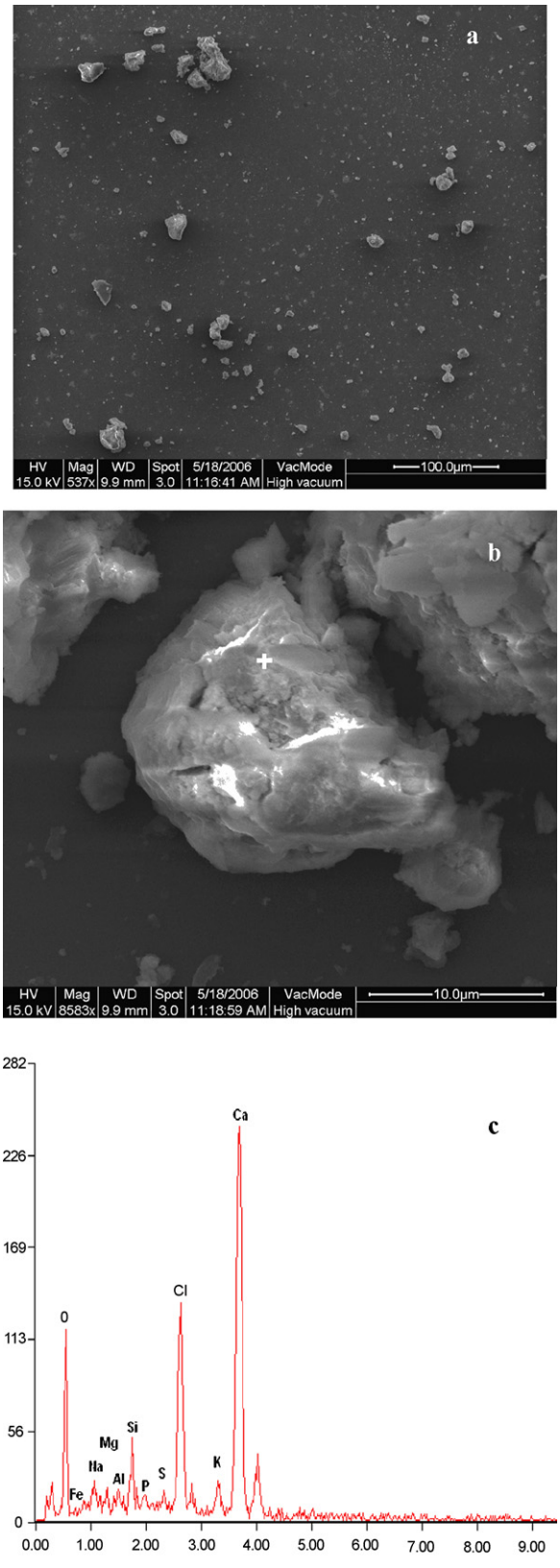

Fig. 4. SEM and EDS image of SRFA600.

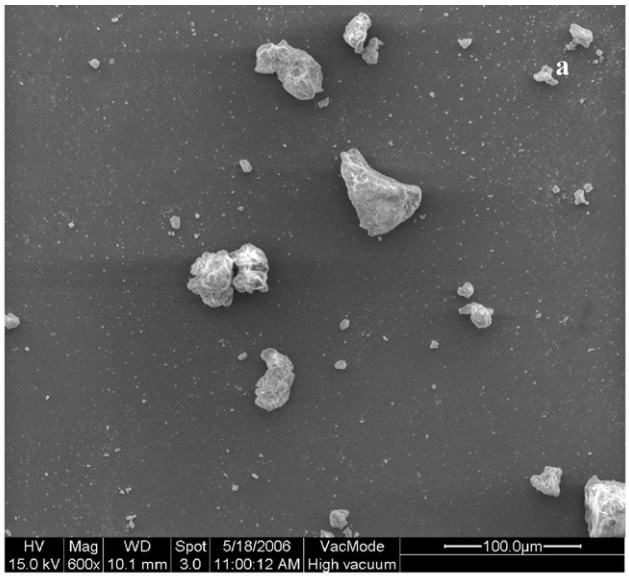

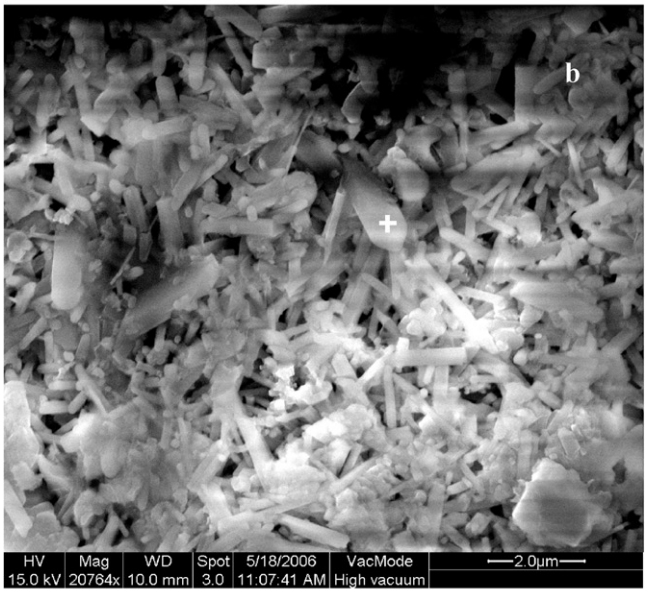

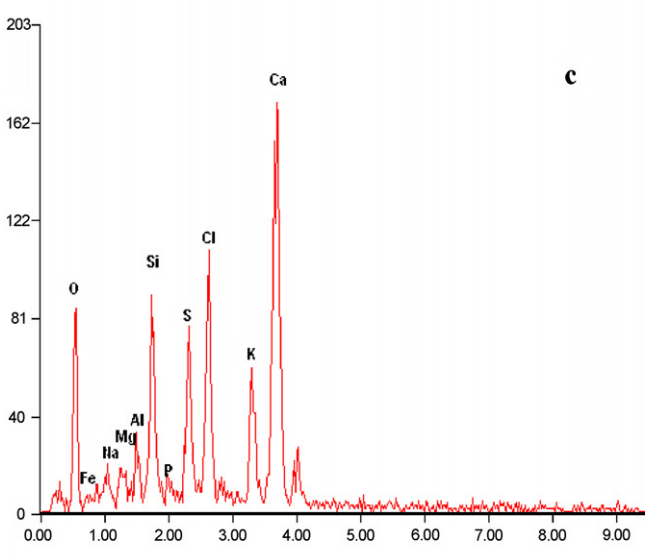

Fig. 5. SEM and EDS image of SRFA700.

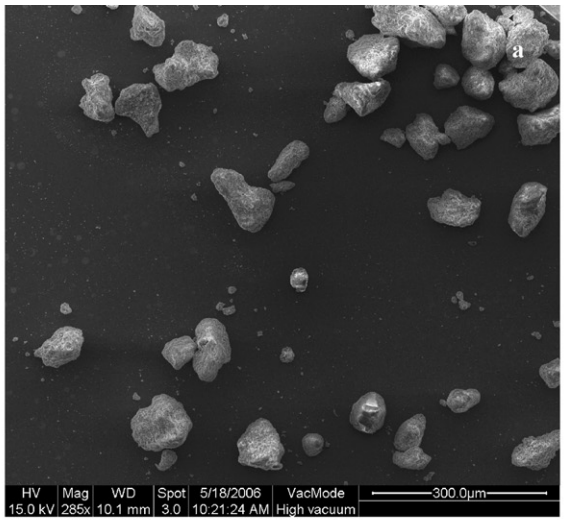

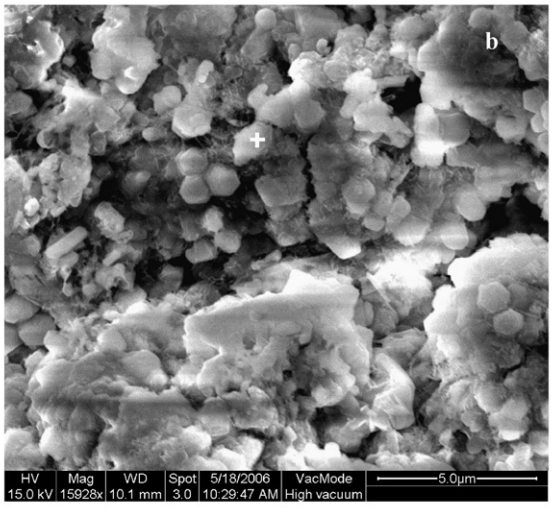

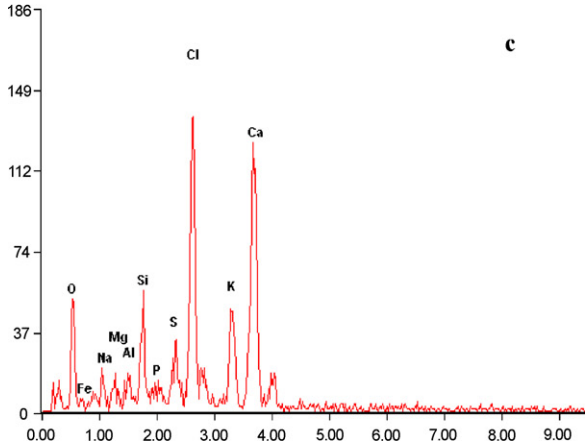

Fig. 6. SEM and EDS image of SRFA800.

species below 0.1% cannot be identified from background noise regardless of FOM.

The SEM–EDS (Quanta 200F, FEI; Genesis, EDAX) was employed to provide detailed imaging information about the morphology and surface texture of individual particles, as well as composition of the powder samples.

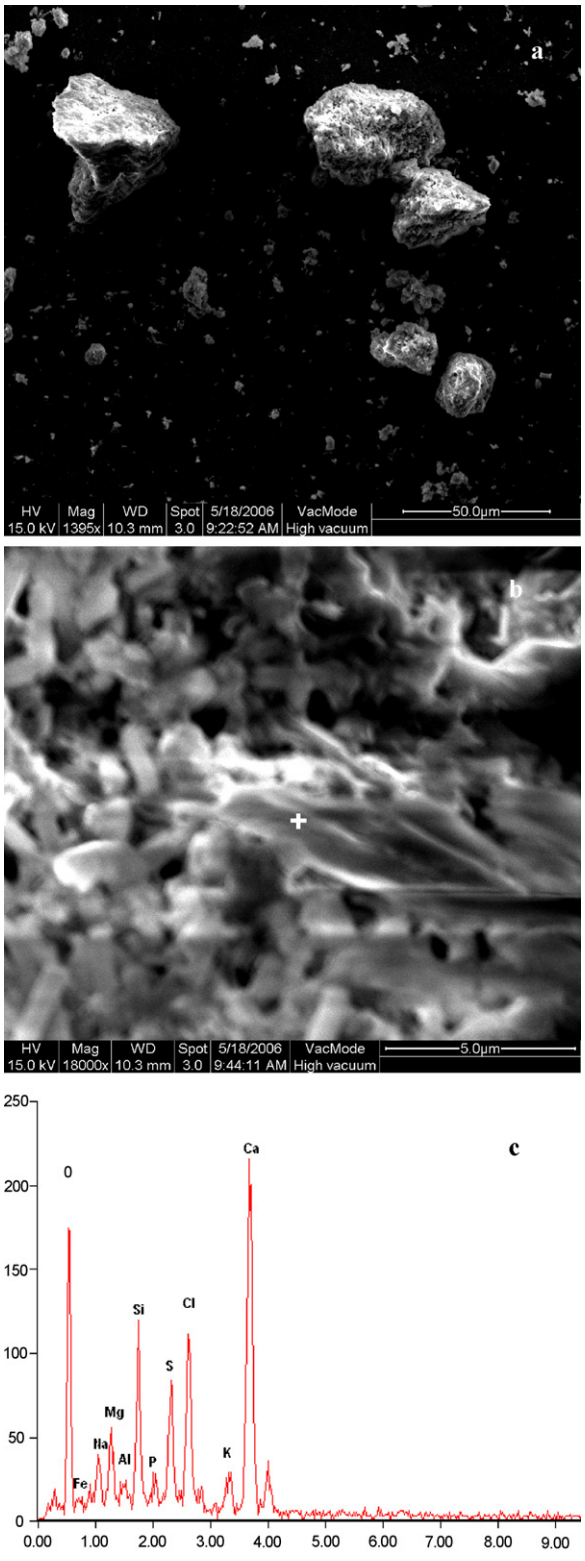

Fig. 7. SEM and EDS image of SRFA900.

In the TCLP experiments, concentrations of Cu, Cr, Cd, Pb, Zn and Ni were determined by atomic absorption spectroscopy (AAS) using direct aspiration, which was described in Liu et al. [12,13]. The detection limits for Cd, Cr, Pb, Zn, Cu, and Ni were, respectively, 3, 50, 100, 5, 20, and 40 $\mu g\,L^{-1}$.

3. Results and discussion

3.1. Characterization of MSWI fly ash

The elemental composition of the baghouse fly ash used in this study is summarized in Table 1. It is noted that Ca and Cl, accounting for 23.39% and 15.82%, respectively, were the major elements found in the tested fly ash. The $Ca(OH)_2$ solution sprayed in the semi-dry scrubber resulted in the high concentration of Ca in this fly ash.

Na, S, K, Si, Al, Mg and Fe were the next most abundant elements, each comprising about 1–6%. Heavy metals Zn, Cr, Pb and Cu comprised about 0.16–0.91%, whereas Cd and Ni only about 0.021–0.025%.

3.2. Microstructure of RFA and sintered products

The raw fly ash was sintered at 500 °C, 600 °C, 700 °C, 800 °C and 900 °C for 1 h, and then the corresponding sintered products SRFA500, SRFA600, SRFA700, SRFA800 and SRFA900 were obtained. Fig. 1 shows the XRD patterns of RFA powder and its sintered products.

Comparisons of the diffractograms, the number of peaks identified by the integrator, the principal minerals identified by the search-match program, and the number of peaks left unresolved by the search-match program indicated that the three replicates gave very comparable information [11]. The spectra was very complex, usually containing 40–60 peaks. A computerized search-match routine was employed as a first step in crystalline mineral identification. The probable minerals should be present in at least two of the three replicates, and have low FOM value (generally 20 or less). All the probable aluminosilicates emerging in RFA powder and the sintered products are summarized in Table 2 and illustrated in Fig. 1.

The XRD patterns (Fig. 1) revealed that with an increase of sintering temperature, more complex aluminosilicates were newly formed, especially in SRFA900. In RFA, anorthite ($CaAl_2Si_2O_8$) was found to be the only aluminosilicate with an FOM below 20; this mineral was also observed by Eighmy et al. [11] in the electrostatic precipitator ash. Many Ca-containing minerals were identified with XRD, for example, Anhydrite ($CaSO_4$), CaClOH, $KCaCl_3$, $CaCl_2(H_2O)_4$, and $Ca(OH)_2$, due to the lime spray for acidic gas removal in the spray-dryer system.

Zoisite ($Ca_2Al_3Si_3O_{11}(O,OH)_2$) and gehlenite ($Ca_2Al_2SiO_7$) emerged in SRFA500. Grossular ($Ca_3Al_2(SiO_4)_2(OH)_4$) was present in SRFA600, SRFA700 and SRFA900, but it could not be found in SRFA900. Besides grossular, the major aluminosilicates in SRFA600 and SRFA700 were zoisite and hibschite ($Ca_3Al_2(SiO_4)_{1.25}(OH)_7$), respectively. When the sintering temperature reached 800 °C, the element Mg was incorporated into the complex aluminosilicates, such as glaucophane ($Na_2Mg_3Al_2Si_8O_{22}(OH)_2$) and cordierite ($Mg_2Al_4Si_5O_{18}$). When the sintering temperature reached 900 °C, the incorporation of Mg and Fe into the aluminosilicates formed new crystalline phases, for example, Ferrotschermakite ($Ca_2Fe_3Al_2(Si_6Al_6)O_{22}(OH)_2$), Ferroglaucophane ($Na_2(Fe,Al,Mg)_5Si_8O_{22}(OH)_2$) and Ferrogedrite ($Fe_5Al_4Si_6O_{22}(OH)_2$).

As shown in Table 2, the number of the minerals (except aluminosilicates) detected by XRD was reduced with an increase of sintering temperature. On the contrary, more complex aluminosilicate was detected with the increased temperature. It is possible that these simple minerals were gradually incorporated into the complex aluminosilicates when the sintering temperature increased. For example, the simple minerals CaClOH, CaO, MgO and FeS_2 was seen in the sintered products with low temperature (SRFA 500 and SRFA600), but they were not detected by XRD in those with higher temperature (SRFA700, SRFA800 and SRFA900). It indicated that the onset of glass formation reactions was about 700 °C for fly ash.

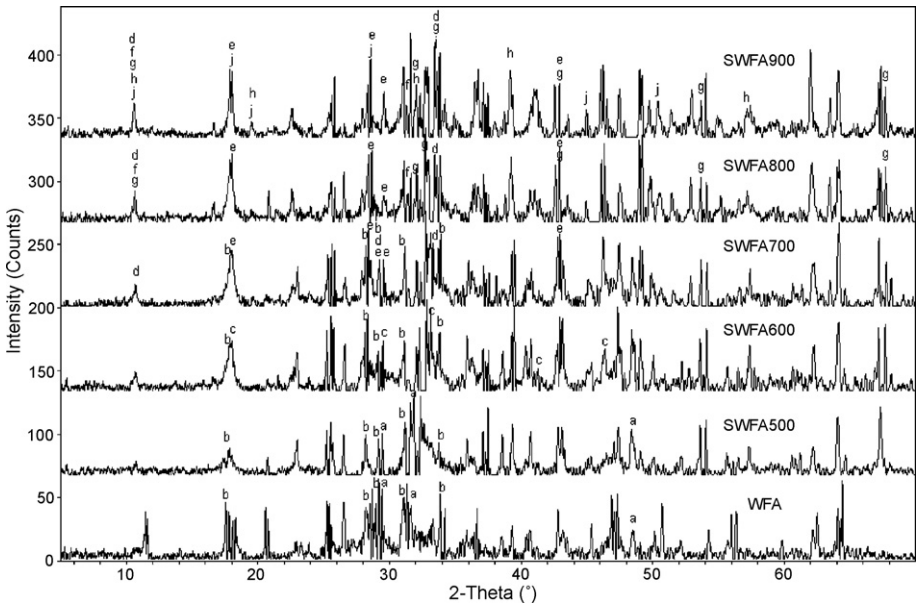

Fig. 8. XRD patterns of WFA powder and its sintered products. (a) Gehlenite, (b) zoisite, (c) grossular, (d) glaucophane, (e) cordierite, (f) ferrogedrite, (g) $Pb_6Al_2Si_6O_{21}$, (h) ferroglaucophane, (j) ferrotschermakite.

Karamanov et al. [2] also found the onset of glass formation reactions occurred at 660 °C for the mixture of 70% fly ash and 30% waste from feldspar production.

Figs. 2–7 illustrate the SEM/EDS observations for RFA and its sintered products at different temperatures. RFA was a kind of loose material with most of finer particles smaller than 0.5 μm and a lesser amount of larger aggregates between 1.0 and 2.0 μm in size (Fig. 2a and b). During sintering process, the loose and fine particles in RFA tended to be aggregated into a significant amount of isolated larger particles (Figs. 3a, 4a, 5a, 6a and 7a). As determined by EDS, the predominant elements in the sintered products at different temperatures were Ca, Si, O, Cl, S, Al, and Mg in various compounds; lesser amounts of the elements Fe, Zn, P, K and Na were also observed.

In SRFA500, large particles were formed like the one depicted in Fig. 3b, which look like an approximate sphere (over 20.0 μm in diameter) with many open pores in its surface. An EDS analysis illustrated that the major constituents for this particle were O, Si, Ca, Zn, Mg, Al and Fe (Fig. 3c). This result was consistent with the XRD data (Table 1) which revealed that Zoisite and gehlenite were the major aluminosilicates, and FeF_2, $Ca_2ZnSi_2O_7$ and MgO were the other principal minerals in SRFA500. Therefore, this large particle was probably the mixture of these aluminosilicates and minerals.

The similar large particles could be found in SRFA600 (Fig. 4b), however, it seemed to be more compact in SRFA600 than in SRFA500. The EDS analysis (Fig. 4c) illustrated that the percentages of the major elements in this particle were much different from those in Fig. 3c. The needle-shaped crystals (over 2 μm in length) were present in SRFA700, while hexagonal crystals were formed in SRFA800. Figs. 5c and 6c show that the needle-shaped crystal consisted of the same elements as the hexagonal crystals; however, the XRD data in Table 2 revealed that the major crystals were grossular ($Ca_3Al_2(SiO_4)_2(OH)_4$) and hibschite ($Ca_3Al_2(SiO_4)_{1.25}(OH)_7$) in SRFA700, while glaucophane ($Na_2Mg_3Al_2Si_8O_{22}(OH)_2$) and Cordierite ($Mg_2Al_4Si_5O_{18}$) in SRFA800. Therefore, the element Mg was possibly incorporated into the hexagonal crystals instead of incorporation into the needle-shaped crystal. Fig. 7b shows that the crystalline phases were slightly molten at 900 °C, and the XRD data (Table 2) illustrated that Fe was incorporated into these crystalline phases.

3.3. Microstructure of WFA and sintered products

The washed fly ash was sintered at 500 °C, 600 °C, 700 °C, 800 °C and 900 °C for 1 h, and then the corresponding sintered materials SWFA500, SWFA600, SWFA700, SWFA800 and SWFA900 were obtained.

Fig. 8 shows the XRD patterns of WFA powder and its sintered products. All the probable aluminosilicates emerging in WFA powder and the sintered products are summarized in Table 3 and illustrated in Fig. 8. All of the FOMs for these aluminosilicates in Table 3 were below 20.

The minerals present in WFA were much different from those in RFA; many of the soluble minerals like CaClOH, $KCaCl_3$ and $CaCl_2(H_2O)_4$ were dissolved. Zoisite and gehlenite were the principal aluminosilicates present in WFA. A lot of hydrates were produced during the washing treatment including $CaSO_4(PO_3OH)_4H_2O$, Hydrocalumite ($Ca_4Al_2O_6Cl_2{\cdot}10H_2O$), and $Na_{12}[Zn_{12}P_{12}O_{48}]{\cdot}12H_2O$ (see Table 3). These hydrates seemed to be the precursor compounds for the complex aluminosilicates formed at the higher sintered temperature, because they were not detected by XRD analysis in all the sintered products.

Zoisite was present in WFA, SWFA500, SWFA600 and SWFA700, but it could not be found in SRFA800 and SWFA900. In WFA and SWFA500, gehlenite could be detected by XRD (FOM < 20), but it was not found in the sintered products at higher temperatures over 600 °C. Glaucophane and cordierite emerged in SWFA700, SWFA800 and SWFA900. When the sintering temperature reached 700 °C, the element Mg was incorporated into the complex aluminosilicates (e.g., glaucophane and cordierite); whereas for the sintered unwashed fly ash, the temperature for the Mg incorporation was 800 °C (Table 2). When the sintering temperature reached 800 °C or more, the incorporation of Mg, Fe and Pb into the aluminosilicates formed new crystalline phases, for example, Ferrogedrite, lead aluminum silicate ($Pb_6Al_2Si_6O_{21}$), Ferrotschermakite, and Ferroglaucophane.

Table 3
XRD-based possible mineralogy of washed fly ash and sintered products

WFA		SWFA500		SWFA600		SWFA700		SWFA800		SWFA900	
Minerals	FOM	Minerals	FOM	Minerals	FOM	Minerals	FOM	Minerals	FOM	Minerals	FOM
Aluminosilicates											
Gehlenite $Ca_2Al_2SiO_7$	13.8	Gehlenite $Ca_2Al_2SiO_7$	18.9	Zoisite $Ca_2Al_3Si_3O_{11}(O,OH)_2$	17.8	Glaucophane $Na_2Mg_3Al_2Si_8O_{22}(OH)_2$	13.1	Glaucophane $Na_2Mg_3Al_2Si_8O_{22}(OH)_2$	17.8	Cordierite $Mg_2Al_4Si_5O_{18}$	11.8
Zoisite $Ca_2Al_3Si_3O_{11}(O,OH)_2$	19.6	Zoisite $Ca_2Al_3Si_3O_{12}OH$	19.5	Grossular $Ca_3Al_2Si_3O_{12}$	18.3	Zoisite $Ca_2Al_3Si_3O_{11}(O,OH)_2$	13.3	$Pb_6Al_2Si_6O_{21}$	18.6	Ferrotschermakite $Ca_2Fe_3Al_2(Si_6Al_6)O_{22}$-$(OH)_2$	12.2
						Cordierite $Mg_2Al_4Si_5O_{18}$	19.2	Ferrogedrite $Fe_5Al_4Si_6O_{22}(OH)_2$	19.2	Glaucophane $Na_2Mg_3Al_2Si_8O_{22}(OH)_2$	12.6
								Cordierite $Mg_2Al_4Si_5O_{18}$	19.8	Ferrogedrite $Fe_5Al_4Si_6O_{22}(OH)_2$	16.4
										Ferroglaucophane $Na_2(Fe,Al,Mg)_5Si_8O_{22}$-$(OH)_2$	18.4
										$Pb_6Al_2Si_6O_{21}$	18.8
										Cummingtonite[a]	19.8
Other major minerals											
Gypsum	6.2	MgO	6.2	$CaSO_4$	13.4	ZnS	10.9	$Na_2Fe^{4+}{}_2Fe^{2+}{}_3Si_6O_{20}$	10.3	Hydroxylellestadite	6.9
$CaSO_4(PO_3OH)_4H_2O$	6.3	$CaCO_3$	9.4	$Ca_3Mg(SiO_4)_2$	15.0	$(Ca,Mn)CO_3$	14.0	$Ca_{10}(SiO_4)_3(SO_4)_3Cl_2$	12.9	$Cd_2SiP_4O_{14}$	13.7
Hydrocalumite $Ca_4Al_2O_6Cl_2{\cdot}10H_2O$	8.5	$(MgO)_{0.91}FeO_{0.09}$	10.7	ZnS	15.5	$CaCO_3$	14.9	Hydroxylellestadite	14.2	$Ca_{10}(SiO_4)_3(SO_4)_3Cl_2$	15.7
$KCdCl_3(H_2O)$	8.7	Gypsum	11.7	$Ca_{15}(PO_4)_2(SiO_4)_6$	15.7	$AlFeO_3$ (84-2153)	11.8	$Ca_{14}Mg_2(SiO_4)_8$	16.8	$Ca_2MgSi_2O_7$	18.2
$KCu_3OCl(SO_4)_2$	9.5	$Ca_5(PO_4)_3(OH,Cl,F)$	18.8	$Ca_2ZnSi_2O_7$	16.8	$Ca_3Al_2O_6$ (32-0148)	15.0	$Ca_3Mg(SiO_4)_2$	17.3	$Ca_{14}Mg_2(SiO_4)_8$	18.8
$Na_{12}[Zn_{12}P_{12}O_{48}]{\cdot}12H_2O$	9.8	$MgCO_3$	19.5	$Ca_3Al_2O_6$	17.2	$Ca_6Zn_3Al_8O_{15}$	18.7	$Ca_5(SiO_4)_2CO_3$	17.7		
AlOCl	10.0	$Ca_2ZnSi_2O_7$	19.5	$CaCO_3$	18.6	$Ca_2ZnSi_2O_7$	19.5	$Ca_2ZnSi_2O_7$	19.4		
ZnS	10.8	Zn_2SiO_4	19.7								
FeOCl	12.5	$(Mg,Fe)_2SiO_4$	19.7								
$Ca_2Al(OH)_6Cl{\cdot}2H_2O$	13.2	Na_4SiO_4	19.7								
$CaSi_2O_5$	13.8	$CaSO_4$	19.8								
$Ca_{10}Si_5O_{18}(Cl,OH)_4$	14.6										
$Ca_2ZnSi_2O_7$	15.8										
Hydroxylellestadite	16.1										
$Mg_2Si_2O_6$	16.1										
$Mg(OH)_2$	16.5										
Zn_2SiO_4	18.1										
$Ca_5Si_2O_7(CO_3)_2$	18.4										
SiO_2	18.8										
$Ca(OH)_2$	19.5										
$Ca_2MgSi_2O_7$	19.8										

[a] Cummingtonite (PDF-#: 86-0159): $[Fe_{2.558}Mg_{4.344}Ca_{0.086}Al_{0.012}][Si_8O_{22.012}(OH)_{1.988}]$.

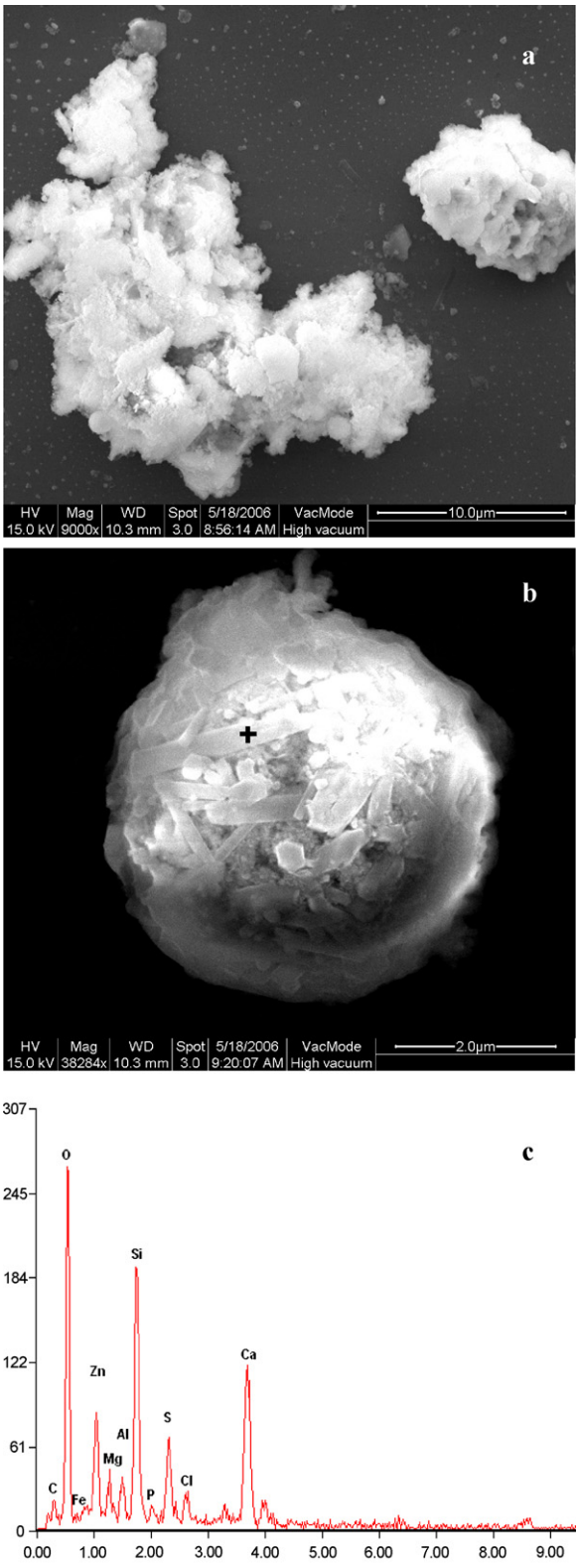

Fig. 9. SEM and EDS image of WFA.

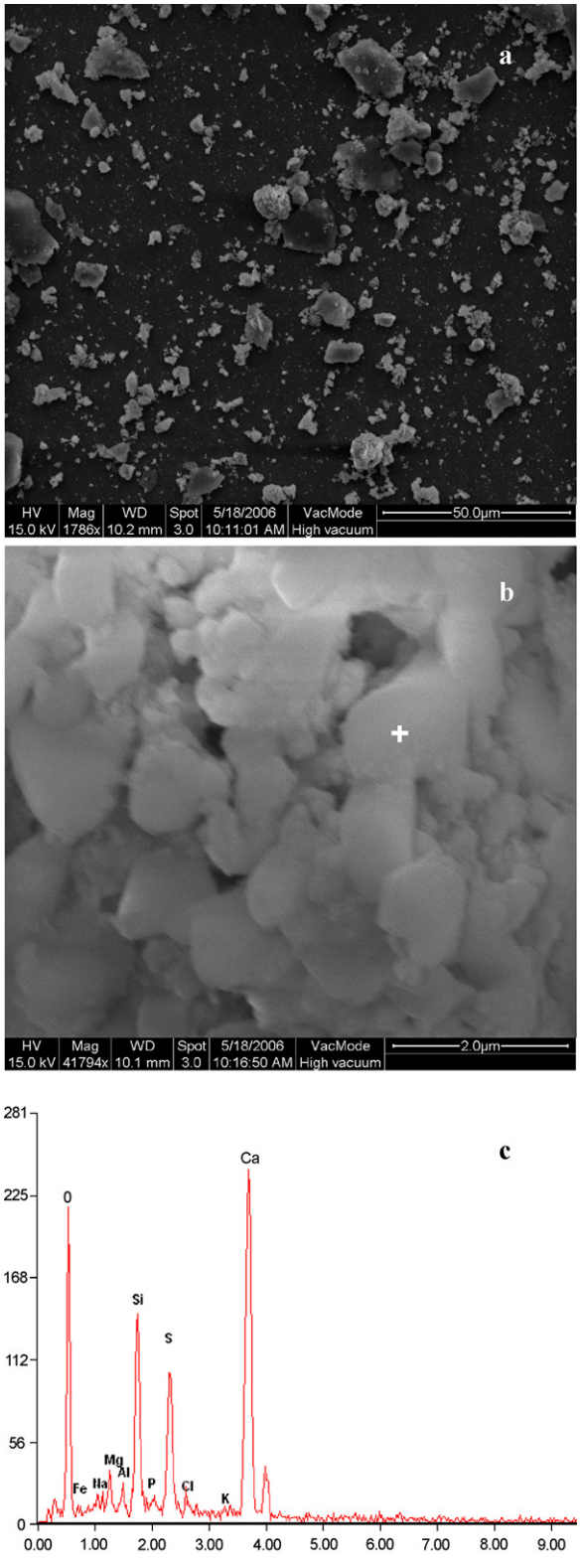

Fig. 10. SEM and EDS image of SWFA500.

For the unwashed fly ash, the element Fe was only incorporated into the aluminosilicates at 900 °C, and Pb was not found to be incorporated into the aluminosilicates according to XRD analysis. Therefore, the washing process produced significant effects on crystal formation. In the higher sintering temperature (800 and 900 °C), major aluminosilicates were found to be identical in the sintered products. For example, Glaucophane and cordierite were present in SRFA800 and SWFA800, and glaucophane, cordierite, ferrogedrite, ferroglaucophane and ferrotschermakite were all observed in SRFA900 and SWFA900. Except these complex aluminosilicates, the

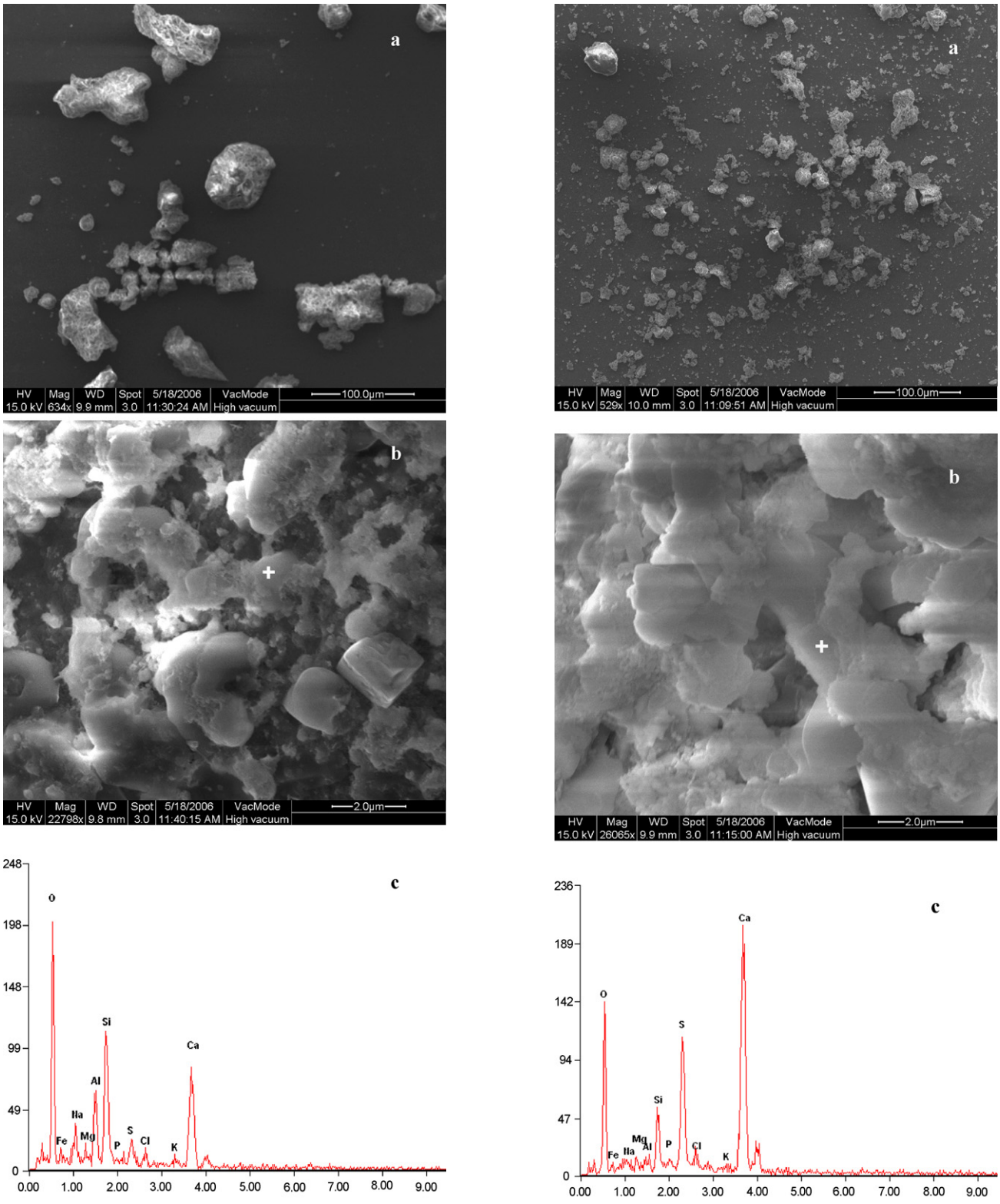

Fig. 11. SEM and EDS image of SWFA600.

Fig. 12. SEM and EDS image of SWFA700.

other major minerals in the sintered RFA products were significantly different from those in the sintered WFA products at the same sintering temperature (Tables 2 and 3).

Figs. 9–14 illustrated the SEM/EDS observations for WFA and its sintered products at different temperatures. The fracture surface morphology of washed fly ash (Fig. 9) was much different from that of raw fly ash (Fig. 2). Many hydrates produced in the washing treatment formed large aggregates, some of which was over 40 μm in diameter (Fig. 9b). As determined by EDS, the predominant elements in WFA were Ca, S, Si, Zn, O, Al and Mg. Due to the high solubility in water, most of the chlorides were removed by the washing treatment [9]; the content of Cl in WFA was very low,

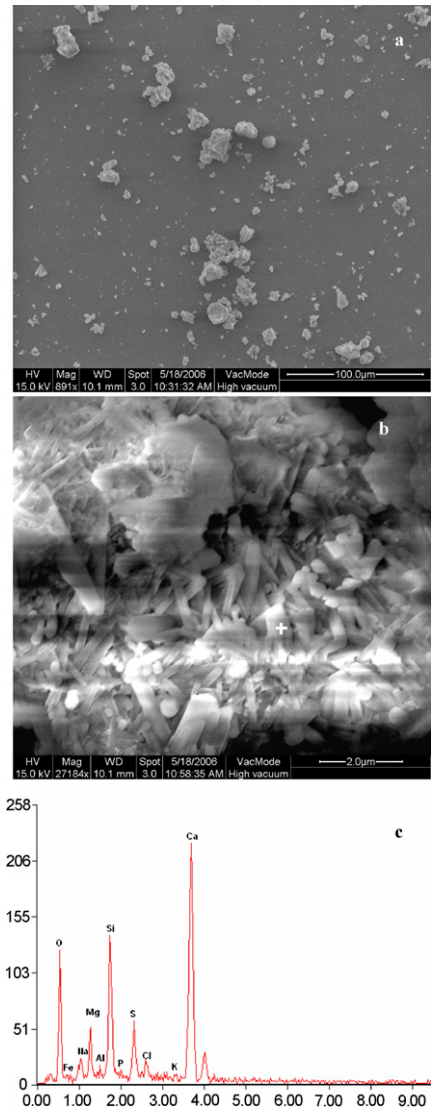

Fig. 13. SEM and EDS image of SWFA800.

compared with the raw fly ash (Table 1). According to Table 3, the major compounds containing Zn were $Na_{12}[Zn_{12}P_{12}O_{48}]\cdot 12H_2O$, ZnS, $Ca_2ZnSi_2O_7$ and Zn_2SiO_4. Although the Zn content was as much as 9043 mg kg^{-1} in the raw fly ash (Table 1), the XRD could not detect crystalline minerals containing Zn with FOM below 20 (Table 2).

During sintering process, the loose particles in WFA tended to be aggregated into a great deal of larger particles (Figs. 10a, 11a, 12a, 13a and 14a). This phenomenon was also found for the unwashed fly ash during the sintering process. The EDS analysis (Figs. 10c, 11c, 12c, 13c and 14c) showed that the predominant elements in the sintered products at different temperatures were Ca, Si, O, S, Al, and Mg in various compounds; lesser amounts of the elements Fe, Zn, P, Cl, K and Na were also observed. The contents of Cl in the sintered products of washed fly ash were significantly lower than those in the sintered raw fly ash products.

The elongated crystals present in WFA (Fig. 9b) were converted into the "smooth" particles with larger pores in SWFA500, SWFA600 and SWFA700 (Figs. 10b, 11b and 12b). The needle-shaped crystals were present in SWFA800, which was also found in SRFA700. However, almost no identical minerals were found except $Ca_2ZnSi_2O_7$ in SRFA700 and SWFA800. The crystalline phases in SWFA900 did not melt in the same way as SRFA900.

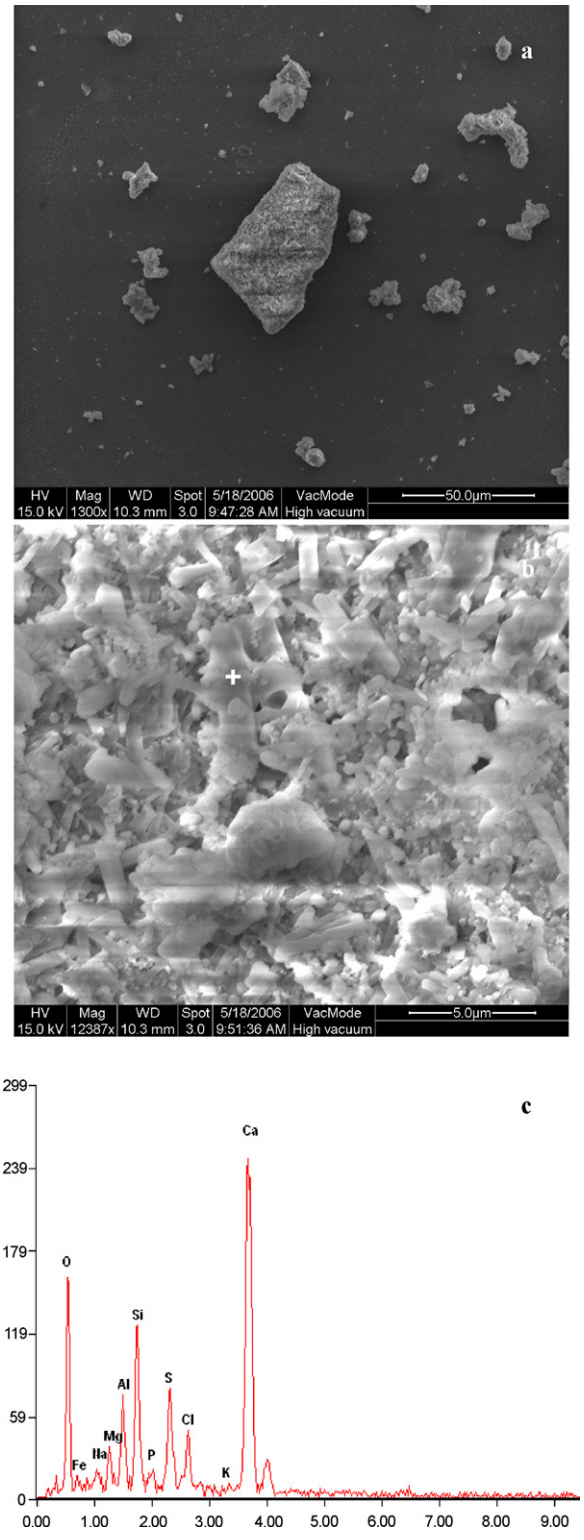

Fig. 14. SEM and EDS image of SWFA900.

3.4. Effect of sintering temperature on heavy metal leachability

Fig. 15 illustrates the leachate concentration of heavy metals (Cr, Cd, Pb, Cu, Ni and Zn) from RFA, WFA and their sintered products.

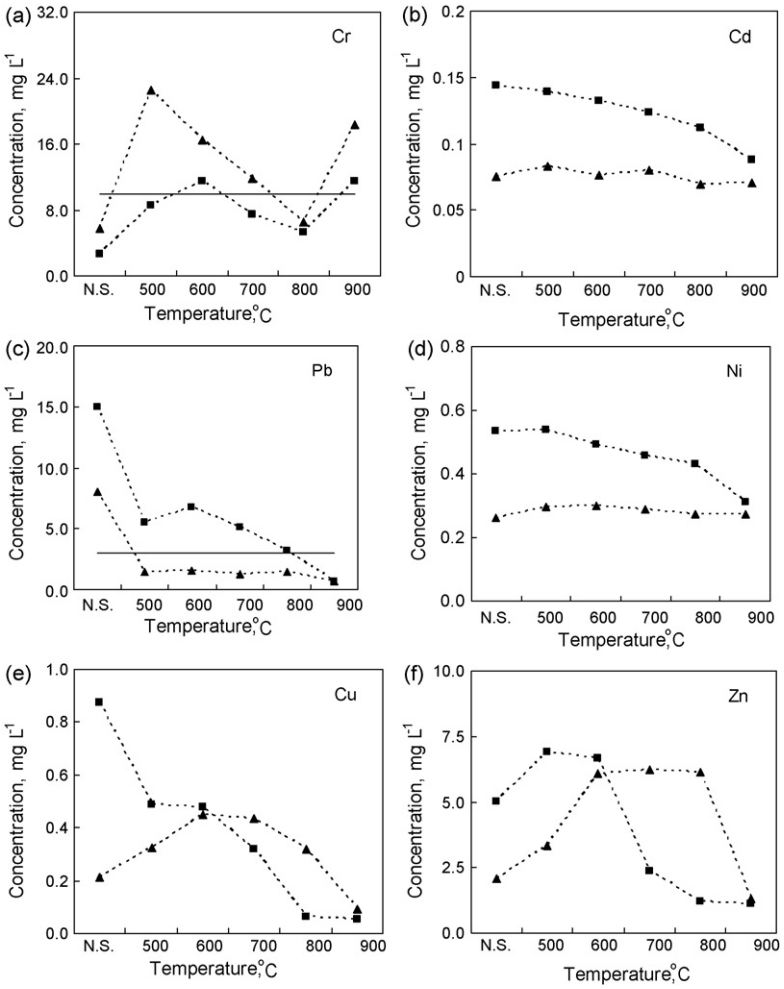

Fig. 15. Effect of sintering temperature on the leachate concentrations of heavy metals. (▲)-Washed fly ash, (■)-raw fly ash. N.S.-not sintered, which referred to RFA and WFA. The solid lines in (a) and (c) showed the regulatory limits for Cr and Pb. The regulatory limits for Cd, Ni, Cu and Zn were not shown in their plots because they were much larger than their leachate concentrations.

The Chinese regulatory levels for Cr, Cd, Pb, Cu, Ni and Zn in the leachate were 10, 0.3, 3, 50, 10 and 50 mg L^{-1}, respectively [14]. The leachate concentration of Cd, Cu, Zn and Ni was much below their respective regulatory level in China, no matter from RFA, WFA or their sintered products. The level of Pb leached from WFA and the sintered products of RFA and WFA was below its regulatory level, but for the raw fly ash, the leachate level of Pb exceeded 10 mg L^{-1}, reaching 15 mg L^{-1}.

The leachable content of Cd, Pb and Ni from RFA and its sintered products was higher than that from WFA and the sintered products (Fig. 15b–d). Therefore, the washing treatment reduced the leachable concentration of these heavy metals. As shown in Fig. 15e and f, Zn and Cu tended to be more leachable in the raw fly ash than in the washed fly ash when the sintering temperature was no more than 600 °C; however, when the sintering temperature reached 700 °C or more, the leachate concentration of Cu and Zn was greater from washed fly ash than from the raw fly ash. Correspondingly, the washing treatment made Zn and Cu more leachable at higher sintering temperature over 700 °C.

It seemed that Cr tended to be more leachable from WFA than from RFA. Similarly, the leachate concentration of Cr was greater from the sintered products of washed fly ash than from the sintered raw fly ash at the same temperature. Therefore, Cr appears to become more soluble after the washing treatment.

For the raw fly ash, Fig. 15a shows that the leachate concentration of Cr increased remarkably with sintering temperature and reached the concentration value of 11.46 mg L^{-1} at 600 °C, and then fell gradually to the concentration value of 5.34 mg L^{-1} at 800 °C; finally, it increased dramatically, reaching 11.51 mg L^{-1} at 900 °C. The Cr leaching concentration from all the sintered products of washed fly ash was higher than that from the raw fly ash by 2.0–4.3 times; therefore the thermal treatment made Cr more leachable. For the washed fly ash, Cr leaching as a function of sintering temperature was similar with that for the raw fly ash, but the leachate concentration from the washed fly ash was greater than that from the raw fly ash at the same sintering temperature (Fig. 15a). Many researchers [15,16] also observed that the thermal treatment increased the leachate concentration of Cr from fly ash; however, there was no reference suggesting that the Cr leachable content from the sintered products at different temperature would vary in such a way as illustrated in Fig. 15a.

Wang et al. [8] reported that the increased Cr leaching concentration was attributable to the high-temperature oxidation of the insoluble trivalent chromium (Cr^{3+}) to its soluble hexavalent form (Cr^{6+}). Some Cr (≈12%) was shown to have become soluble and consequently leached from the sintered residue [15]. Kirk et al. [15] found that CaO and $CaCl_2$ present in the fly ash could increase the soluble fraction of Cr up to 54% and 27% in the thermal treatment,

and the XRD analyses revealed the presence of calcium chromate ($CaCrO_4$). This species is soluble and could account for the increase in solubility of the thermally treated Cr compounds in fly ash samples. Therefore, The possible reason for the increased Cr leachable concentration from the sintered products in this study may be related to the oxidation of Cr(III) to Cr(VI) during the sintering treatment, and a $CaCrO_4$ compound could be considered as a potential soluble species.

4. Conclusions

This study investigated the characterization of fly ash and washed fly ash at different sintering temperatures by virtue of SEM/EDS and XRD instruments. The results showed that, the loose and fine particles in RFA and WFA tended to be aggregated into a great deal of larger particles during sintering process; the increased sintering temperature produced more complex aluminosilicates, and the metals Mg, Fe and Pb were incorporated into the newly formed aluminosilicates at higher temperatures over 800 °C. However, due to the complex matrix of fly ash, identification of complex minerals (especially aluminosilicates) based upon the XRD technique and the PC-based search-match program is speculative.

TCLP tests demonstrated that the washing treatment reduced the leachable level of Cd, Pb and Ni, but increased that of Cr. The possible reason for the increased Cr leachable concentration from the sintered products may be related to the oxidation of Cr(III) to Cr(VI) during the sintering treatment, and a $CaCrO_4$ compound could be considered as a potential soluble species. The leachable content of Cd, Cu, Zn and Ni from RFA, WFA or their sintered products was much below their respective regulatory level. The Pb level leached from WFA, SRFA and SWFA was all below its regulatory level, but for the raw fly ash, the leachate level of Pb exceeded 3 mg L^{-1}, reaching 15 mg L^{-1}.

References

[1] Y.S. Shim, S.W. Rhee, W.K. Lee, Comparison of leaching characteristics of heavy metals from bottom and fly ashes in Korea and Japan, Waste Manage. 25 (2005) 473–480.
[2] A. Karamanov, M. Pelino, A. Hreglich, Sintered glass-ceramics from municipal solid waste-incinerator fly ashes—part I: the influence of the heating rate on the sinter-crystallisation, J. Eur. Ceram. Soc. 23 (2003) 827–832.
[3] S. Bethanis, C.R. Cheeseman, C.J. Sollars, Properties and microstructure of sintered incineration bottom ash, Ceram. Int. 28 (2002) 881–886.
[4] Y.J. Park, J. Heo, Vitrification of fly ash from municipal solid waste incinerator, J. Hazard. Mater. 91 (2002) 83–93.
[5] A. Polettini, R. Pomi, L. Trinci, Engineering and environmental properties of thermally treated mixtures containing MSWI fly ash and low cost additives, Chemosphere 56 (2004) 901–910.
[6] S. Sakai, M. Hiraoka, Municipal solid waste incinerator residue recycling by thermal processes, Waste Manage. 20 (2000) 249–258.
[7] R. Derie, A new way to stabilize fly ash from municipal incinerators, Waste Manage. 16 (1996) 711–716.
[8] K.S. Wang, K.Y. Chiang, K.L. Lin, C.J. Sun, Effects of a water-extraction process on heavy metal behavior in municipal solid waste incinerator fly ash, Hydrometallurgy 62 (2001) 73–81.
[9] G. De Casa, T. Mangialardi, A.E. Paolini, L. Piga, Physical-mechanical and environmental properties of sintered municipal incinerator fly ash, Waste Manage. 27 (2007) 238–247.
[10] Y.S. Liu, S.D. Xie, Y.Q. Li, Y.S. Liu, Novel mercury control technology for solid waste incineration: sodium tetrasulfide (STS) as mercury capturing agent, Environ. Sci. Technol. 41 (2007) 1735–1739.
[11] T.T. Eighmy, J.D.J.R. Eusden, J.E. Krzanowski, D.S. Domingo, D. Stämpfli, J.R. Martin, P.M. Erickson, Comprehensive approach toward understanding element speciation and leaching behavior in municipal solid waste incineration electrostatic precipitator ash, Environ. Sci. Technol. 29 (1995) 629–646.
[12] Y.S. Liu, L.L. Ma, Y.S. Liu, G.X. Kong, Investigation of novel incineration technology for hospital waste, Environ. Sci. Technol. 40 (2006) 6411–6417.
[13] Y.S. Liu, Y.S. Liu, A novel incineration technology integrated with drying, pyrolysis, gasification and combustion of MSW and ashes vitrification, Environ. Sci. Technol. 39 (2005) 3855–3863.
[14] Chinese EPA, China Identification Standard for Hazardous Waste Toxicity (GB5085.3-1996), Chinese Environmental Science Press, Beijing, 1996.
[15] D.W. Kirk, C.C.Y. Chan, H. Marsh, Chromium behavior during thermal treatment of MSW fly ash, J. Hazard. Mater. 7 (2002) 39–49.
[16] K.S. Wang, C.J. Sun, C.Y. Liu, Effects of the type of sintering atmosphere on the chromium leachability of thermal-treated municipal solid waste incinerator fly ash, Waste Manage. 21 (2001) 85–91.